

The cancellation of spurious arrivals in Green's function extraction and the generalized optical theorem

Roel Snieder⁽¹⁾, Kasper van Wijk⁽²⁾, and Matt Haney⁽³⁾

(1) *Center for Wave Phenomena and Dept. of Geophysics, Colorado School of Mines, Golden CO 80401, email rsnieder@mines.edu*

(2) *Physical Acoustics Laboratory and Dept. of Geosciences, Boise State University, Boise ID 83725*

(3) *USGS Alaska Volcano Observatory, Anchorage AK 99508*

ABSTRACT

The extraction of the Green's function by cross-correlation of waves recorded at two receivers nowadays finds much application. We show that for an arbitrary isolated scatterer, the cross-terms of scattered waves give an unphysical wave with an arrival time that is independent of the source position. This constitutes a paradox because theory predicts that such spurious arrivals do not arise, after integration over a complete source aperture. The paradox can be resolved by integrating the contribution of all sources in the stationary phase approximation to show that the stationary phase contributions to the source integral cancel the spurious arrival by virtue of the generalized optical theorem. This work constitutes an alternative derivation of this theorem. When the source aperture is not complete, the spurious arrival is not canceled and could be misinterpreted to be part of the Green's function.

Key words: interferometry, Green's function extraction

1 INTRODUCTION

In recent years the extraction of the Green's function from field fluctuations has received considerable attention. This technique is described in recent tutorials [Curtis *et al.*, 2006; Larose *et al.*, 2006], and is in the seismic community known as *seismic interferometry*. The Green's function can be retrieved by cross-correlating the fields recorded at two receivers. This approach can be used to extract the impulse response from field fluctuations from thermal noise exciting elastic waves [Weaver & Lobkis, 2001], from oceanic noise exciting surface waves [Shapiro *et al.*, 2005; Sabra *et al.*, 2005], from turbulent flow over an airfoil [Sabra *et al.*, 2008], from chaotic earthquake signals [Snieder & Şafak, 2006; Mehta *et al.*, 2007], or from skeletal muscle noise [Sabra *et al.*, 2007]. Alternatively, one can use controlled

sources. In this case the advantage of extracting the impulse response from cross-correlation lies in the removal of the imprint of medium complexity between the sources and the receivers [Bakulin & Calvert, 2006], or in a more optimal illumination of the target [van Wijk, 2006; Hornby & Yu, 2007].

Even though the theory of Green's function extraction is well-developed and numerous applications have been implemented, there are puzzling open questions; this work presents one of those questions. The Green's function G can be extracted by cross-correlating field fluctuations in two locations \mathbf{r}_A and \mathbf{r}_B . In the frequency domain the expression (21) of ref. [Wapenaar

& Fokkema, 2006] is:

$$\oint \frac{1}{\rho(\mathbf{r})} (G^*(\mathbf{r}_B, \mathbf{r}) \nabla G(\mathbf{r}_A, \mathbf{r}) - G(\mathbf{r}_A, \mathbf{r}) \nabla G^*(\mathbf{r}_B, \mathbf{r})) \cdot \hat{\mathbf{n}} dS$$

$$= 2i \text{Im} (G(\mathbf{r}_A, \mathbf{r}_B)), \quad (1)$$

where $\rho(\mathbf{r})$ is the density, $\hat{\mathbf{n}}$ is the normal outward on the integration surface. For sources far from the receivers ($r \gg r_{(A,B)}$) the Green's function satisfies a radiation boundary condition, so that for a spherical surface with a normal vector in the radial direction $\nabla G(\mathbf{r}_{A,B}, \mathbf{r}) = ikG(\mathbf{r}_{A,B}, \mathbf{r})\hat{\mathbf{n}}$. Using this radiation boundary condition gives, for a constant wave-number and density on the surface:

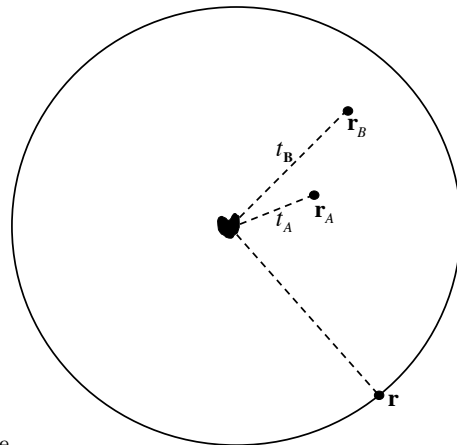
$$\oint G(\mathbf{r}_A, \mathbf{r}) G^*(\mathbf{r}_B, \mathbf{r}) dS = -\frac{\rho}{k} \text{Im} (G(\mathbf{r}_A, \mathbf{r}_B)), \quad (2)$$

where k is the wavenumber and Im denotes the imaginary part. Expression (2) is applicable for the case of acoustic waves treated here. By replacing ρ/k in the right hand side by $k\hbar^2/m$, the analysis is equally applicable to quantum mechanics [Snieder *et al.*, 2007]. The imaginary part of the Green's function can be written as the sum of the Green's function and its complex conjugate, which corresponds in the time domain to the superposition of the causal and a-causal Green's function. This reflects the well-known fact that the cross-correlation leads to the superposition of the causal Green's function and its a-causal counterpart (e.g., [Wapenaar *et al.*, 2005; Lobkis & Weaver, 2001]). Expression (2) forms the basis for the Green's function retrieval from the cross-correlation of waves excited by uncorrelated sources on a closed surface surrounding the observation points [Wapenaar *et al.*, 2005]. A similar relation is valid for open systems where the surface integration needs to be replaced by an integration over all angles of incidence [Weaver & Lobkis, 2004]. Expression (2) contains a surface integral. The counterpart of this expression for general linear systems contains a volume integral as well [Wapenaar *et al.*, 2006; Snieder *et al.*, 2007; Weaver, 2008].

According to equation (2), the Green's function can be found by cross-correlating the waves excited by sources on a closed surface. We present in section 2 a paradox that suggests that unphysical arrivals arise from expression (2). We resolve this paradox in section 3, and illustrate this with a numerical example in the subsequent section. This work is not only of academic interest, we discuss the implications for practical applications of the Green's function retrieval in the conclusion. Details of the employed stationary phase approximations are shown in an appendix.

2 A PARADOX

We consider the special case of an isolated scatterer as shown in figure 1 with scattering amplitude $f_k(\hat{\mathbf{n}}, \hat{\mathbf{n}}')$



centerline
Figure 1. The correlation of scattered waves traveling to points \mathbf{r}_A and \mathbf{r}_B give an arrival at time $t_A - t_B$ for every source point \mathbf{r} .

for incident waves with wavenumber k traveling in the $\hat{\mathbf{n}}'$ -direction that are scattered in the $\hat{\mathbf{n}}$ -direction. The scatterer may have a finite extent and does not need to be either isotropic or weak. The subsequent analysis is in the frequency domain, and, because k is constant at a fixed frequency, we suppress the subscript k in the following.

The scattered waves travel over a time t_A from the scatterer to the receiver at \mathbf{r}_A and in a time t_B from the scatterer to the receiver at \mathbf{r}_B . The Green's function contains a scattered wave that propagates from \mathbf{r}_A via the scatterer to \mathbf{r}_B . The arrival time of this scattered waves is given by the *sum* $t_A + t_B$. The cross-correlation of these waves gives, in the time domain, a wave arriving at the *difference* of these arrivals times, hence it gives after cross-correlation a wave arriving at time at $t_A - t_B$. Note that this time difference is the same for any source location \mathbf{r} . Following this argument, the correlation of the scattered waves in expression (2) gives a wave arriving at a time $t_A - t_B$ at which no physical wave arrives. We call such a wave a *spurious arrival*. Since this arrival has the same travel time for all source positions \mathbf{r} it appears that there is no reason why this arrival vanishes by averaging over all source positions. In the following section we investigate this paradox by a detailed evaluation of the integral in expression (2).

3 STATIONARY PHASE EVALUATION OF THE INTEGRAL

In our analysis we follow the treatment of van der Hulst [van de Hulst, 1949] and assume sources far away ($r \gg r_{A,B}$), consistent with our assumption in equation (2). This makes it possible to evaluate the surface integral with the stationary phase analysis. The stationary phase approximation is exact in the limit $r \rightarrow \infty$. The waves

excited by a point source at \mathbf{r} recorded at locations $\mathbf{r}_{A,B}$ is given by

$$G(\mathbf{r}_A, \mathbf{r}) = -\frac{\rho}{4\pi} \frac{e^{ik|\mathbf{r}-\mathbf{r}_A|}}{|\mathbf{r}-\mathbf{r}_A|} - \frac{\rho}{4\pi} \frac{e^{ikr}}{r} f(\hat{\mathbf{r}}_A, -\hat{\mathbf{r}}) \frac{e^{ikr_A}}{r_A}, \quad (3)$$

$$G(\mathbf{r}_B, \mathbf{r}) = -\frac{\rho}{4\pi} \frac{e^{ik|\mathbf{r}-\mathbf{r}_B|}}{|\mathbf{r}-\mathbf{r}_B|} - \frac{\rho}{4\pi} \frac{e^{ikr}}{r} f(\hat{\mathbf{r}}_B, -\hat{\mathbf{r}}) \frac{e^{ikr_B}}{r_B}. \quad (4)$$

The cross correlation of these fields corresponds, in the frequency domain, to

$$\begin{aligned} & \oint G(\mathbf{r}_A, \mathbf{r}) G^*(\mathbf{r}_B, \mathbf{r}) dS \\ &= \underbrace{\frac{\rho^2}{(4\pi)^2} \oint \frac{\exp(ik(|\mathbf{r}-\mathbf{r}_A| - |\mathbf{r}-\mathbf{r}_B|))}{|\mathbf{r}-\mathbf{r}_A| |\mathbf{r}-\mathbf{r}_B|} dS}_{T1} \\ &+ \underbrace{\frac{\rho^2}{(4\pi)^2} \oint \frac{\exp(ik(|\mathbf{r}-\mathbf{r}_A| - r - r_B))}{|\mathbf{r}-\mathbf{r}_A| r r_B} f^*(\hat{\mathbf{r}}_B, -\hat{\mathbf{r}}) dS}_{T2} \\ &+ \underbrace{\frac{\rho^2}{(4\pi)^2} \oint \frac{\exp(-ik(|\mathbf{r}-\mathbf{r}_B| - r - r_A))}{|\mathbf{r}-\mathbf{r}_B| r r_A} f(\hat{\mathbf{r}}_A, -\hat{\mathbf{r}}) dS}_{T3} \\ &+ \underbrace{\frac{\rho^2}{(4\pi)^2} \oint \frac{\exp(ik(r_A - r_B))}{r^2 r_A r_B} f(\hat{\mathbf{r}}_A, -\hat{\mathbf{r}}) f^*(\hat{\mathbf{r}}_B, -\hat{\mathbf{r}}) dS}_{T4} \end{aligned} \quad (5)$$

The term $T1$ represents the cross-terms of the direct waves at the two receivers, the terms $T2$ and $T3$ represent cross-terms of the direct wave and a scattered wave, while the term $T4$ accounts for the cross-term of the scattered waves. Note that for the latter term the phase is for every integration point \mathbf{r} given by $\exp(ik(r_A - r_B))$, hence it is this term that corresponds, in the time domain, to the spurious arrival at time $t_A - t_B$.

We carry out the surface integrals using a system of spherical coordinates as shown in figure 2. Without loss of generality we use a coordinate system with the scatterer centered on the origin and where the points \mathbf{r}_A and \mathbf{r}_B are located in the (x, z) -plane with $x_B > x_A$ and $z_B > z_A$. In this coordinate system:

$$\begin{aligned} \mathbf{r}_A &= r_A \begin{pmatrix} \sin \theta_A \\ 0 \\ \cos \theta_A \end{pmatrix}, \\ \mathbf{r}_B &= r_B \begin{pmatrix} \sin \theta_B \\ 0 \\ \cos \theta_B \end{pmatrix}, \\ \mathbf{r} &= \begin{pmatrix} \sin \theta \cos \varphi \\ \sin \theta \sin \varphi \\ \cos \theta \end{pmatrix}. \end{aligned} \quad (6)$$

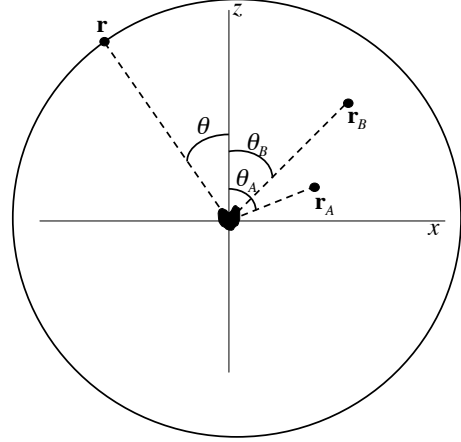


Figure 2. Definition of geometric variables.

For sources located far away ($r \gg r_{A,B}$), this gives to first order in $r_{A,B}/r$:

$$|\mathbf{r} - \mathbf{r}_{A,B}| = r - r_{A,B} (\cos \varphi \sin \theta \sin \theta_{A,B} + \cos \theta \cos \theta_{A,B}). \quad (7)$$

We use this approximation in the exponents of expression (5) while we replace $|\mathbf{r} - \mathbf{r}_{A,B}|$ in the denominators by r . With these replacements the incoming waves effectively are plane waves, which make our analysis applicable for the treatment of the extraction of the Green's function from incoming plane waves [Weaver & Lobkis, 2004] as well. The surface integral is related to an integration over solid angle by the relation $dS = r^2 d\Omega$. Making these simplifications, expression (5) reduces to

$$\begin{aligned} & \oint G(\mathbf{r}_A, \mathbf{r}) G^*(\mathbf{r}_B, \mathbf{r}) dS \\ &= \underbrace{\frac{\rho^2}{(4\pi)^2} \oint \exp(ikL_1) d\Omega}_{T1} \\ &+ \underbrace{\frac{\rho^2}{(4\pi)^2} \oint \frac{\exp(ikL_2)}{r_B} f^*(\hat{\mathbf{r}}_B, -\hat{\mathbf{r}}) d\Omega}_{T2} \\ &+ \underbrace{\frac{\rho^2}{(4\pi)^2} \oint \frac{\exp(-ikL_3)}{r_A} f(\hat{\mathbf{r}}_A, -\hat{\mathbf{r}}) d\Omega}_{T3} \\ &+ \underbrace{\frac{\rho^2}{(4\pi)^2} \frac{\exp(ik(r_A - r_B))}{r_A r_B} \oint f(\hat{\mathbf{r}}_A, -\hat{\mathbf{r}}) f^*(\hat{\mathbf{r}}_B, -\hat{\mathbf{r}}) d\Omega}_{T4}, \end{aligned} \quad (8)$$

with

$$L_1 = |\mathbf{r} - \mathbf{r}_A| - |\mathbf{r} - \mathbf{r}_B|, \quad (9)$$

$$L_2 = |\mathbf{r} - \mathbf{r}_A| - r - r_B, \quad (10)$$

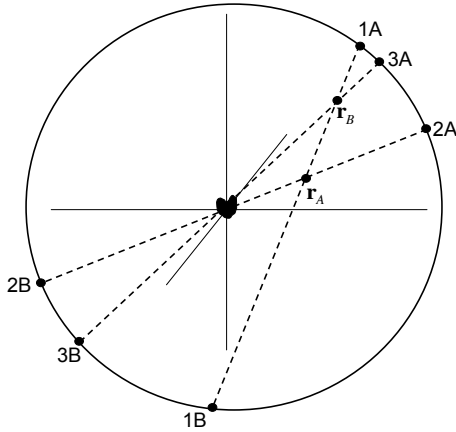


Figure 3. Stationary points in the surface integral of different terms.

$$L_3 = |\mathbf{r} - \mathbf{r}_B| - r - r_A. \quad (11)$$

The term T_4 in expression (8) can be integrated without having to account for phase terms. The other terms have phase terms that we analyze using the stationary phase approximation. The stationary points of the integrals T_1 – T_3 are derived in appendix A. The stationary points are located in the plane of the receivers, the (x, z) -plane for the used coordinate system, and are sketched in figure 3.

The term T_1 has two stationary phase points, indicated with the labels $1A$ and $1B$ on opposite ends of the line through \mathbf{r}_A and \mathbf{r}_B . Physically, the stationary phase point $1A$ gives a direct wave that propagates to \mathbf{r}_B and then continues along a straight path to \mathbf{r}_A . As shown in the appendix, the stationary phase contribution from this point to term T_1 gives

$$T_{1A} = -\frac{i\rho^2}{8\pi k} \frac{\exp(ik|\mathbf{r}_B - \mathbf{r}_A|)}{|\mathbf{r}_B - \mathbf{r}_A|} = \frac{i\rho}{2k} G_0(\mathbf{r}_A, \mathbf{r}_B), \quad (12)$$

where G_0 is the Green's function of the homogeneous medium in which the scatterer is embedded. The stationary phase point $1B$ gives after integration a direct wave that propagates in the opposite direction which is the complex conjugate of the contribution from point $1A$:

$$T_{1B} = -\frac{i\rho}{2k} G_0^*(\mathbf{r}_A, \mathbf{r}_B). \quad (13)$$

The stationary point $2A$ from term T_2 corresponds to the correlation of a direct wave that propagates to \mathbf{r}_A with the scattered wave that arrives at \mathbf{r}_B . As shown in the appendix, the contribution of this stationary phase point gives

$$\begin{aligned} T_{2A} &= \frac{i\rho^2}{8\pi k} \frac{\exp(-ik(r_A + r_B))}{r_A r_B} f^*(\hat{\mathbf{r}}_B, -\hat{\mathbf{r}}_A) \\ &= -\frac{i\rho}{2k} G_S^*(\mathbf{r}_B, \mathbf{r}_A). \end{aligned} \quad (14)$$

This term accounts for the complex conjugate of the scattered wave G_S that propagates between the points $(\mathbf{r}_B, \mathbf{r}_A)$.

The stationary phase point $2B$ of term T_2 gives the correlation between the direct wave arriving from that point at location \mathbf{r}_A and a scattered wave that propagates from the stationary phase point $2B$ through the scatterer to \mathbf{r}_B . As shown in the appendix, the contribution of this stationary phase point is given by

$$T_{2B} = -\frac{i\rho^2}{8\pi k} \frac{\exp(ik(r_A - r_B))}{r_A r_B} f^*(\hat{\mathbf{r}}_B, \hat{\mathbf{r}}_A). \quad (15)$$

This term is not a physical arrival because there is no wave that arrives with a phase given by the length difference $r_A - r_B$. Note that the phase of this term is identical to the phase of the spurious arrival T_4 in equation (8).

The contribution of term T_3 is due to the stationary points $3A$ and $3B$ in figure 3 that have the same physical interpretation as the stationary phase contribution of the points $2A$ and $2B$, respectively for term T_2 . Term T_3 follows most simply by interchanging A and B in term T_2 and by taking the complex conjugate. It thus follows from expressions (14) and (15) that

$$T_3 = \frac{i\rho}{2k} G_S(\mathbf{r}_A, \mathbf{r}_B) + \frac{i\rho^2}{8\pi k} \frac{\exp(ik(r_A - r_B))}{r_A r_B} f(\hat{\mathbf{r}}_A, \hat{\mathbf{r}}_B). \quad (16)$$

Taking all contributions into account by summing expressions (12) through (16) with term T_4 from equation (8), using reciprocity ($G(\mathbf{r}_1, \mathbf{r}_2) = G(\mathbf{r}_2, \mathbf{r}_1)$ and $f(\hat{\mathbf{r}}_1, \hat{\mathbf{r}}_2) = f(\hat{\mathbf{r}}_2, \hat{\mathbf{r}}_1)$), and replacing the integration variable $\hat{\mathbf{r}}$ by $-\hat{\mathbf{r}}$ gives

$$\begin{aligned} \oint G(\mathbf{r}_A, \mathbf{r}) G^*(\mathbf{r}_B, \mathbf{r}) dS &= -\frac{\rho}{k} \text{Im}(G(\mathbf{r}_A, \mathbf{r}_B)) \\ &+ \frac{\rho^2 \exp(ik(r_A - r_B))}{4\pi k r_A r_B} \\ &\times \left[-\text{Im}(f(\hat{\mathbf{r}}_A, \hat{\mathbf{r}}_B)) + \frac{k}{4\pi} \oint f(\hat{\mathbf{r}}_A, \hat{\mathbf{r}}) f^*(\hat{\mathbf{r}}_B, \hat{\mathbf{r}}) d\Omega \right], \end{aligned} \quad (17)$$

where $G = G_0 + G_S$ is the sum of the direct and scattered waves.

The last term in expression (17) contains the spurious event discussed in section 2 that, having in the time domain a travel time $t_A - t_B$, does not correspond to a physical arrival. Perhaps surprisingly, there are two terms within the square brackets that arise from different stationary-phase arrivals from the different terms in the cross-correlation. For this spurious arrival to cancel, and to make expression (17) equal to the general relation (2), the terms within the square brackets must vanish, hence:

$$\text{Im}(f(\hat{\mathbf{r}}_A, \hat{\mathbf{r}}_B)) = \frac{k}{4\pi} \oint f(\hat{\mathbf{r}}_A, \hat{\mathbf{r}}) f^*(\hat{\mathbf{r}}_B, \hat{\mathbf{r}}) d\Omega. \quad (18)$$

This relation is known as the *generalized optical theorem* [Heisenberg, 1943; Glauber & Schomaker, 1953; Schiff,

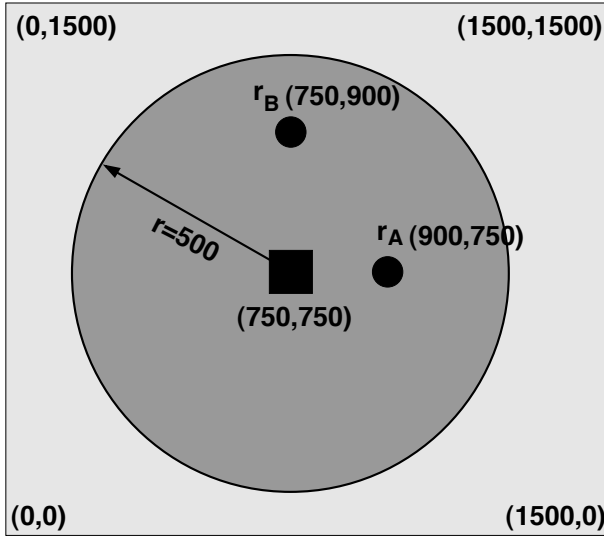


Figure 4. Geometry of the numerical example. The 720 sources are located on a circle with radius 500 m. The scatterer in the origin has dimensions 10 m by 10 m and is not shown to scale. All dimensions are in meters.

1968] which guarantees that the spurious arrivals in expression (17) cancel.

4 NUMERICAL EXAMPLE

We illustrate the cancellation of the spurious arrival with a numerical example based on the Spectral-Element Method. This is a high-order variational numerical technique [Priolo *et al.*, 1994; Faccioli *et al.*, 1997] that combines the flexibility of the finite-element method with the accuracy of global pseudo-spectral techniques. Widely used in seismology [Komatitsch & Tromp, 2002; Komatitsch *et al.*, 2002], we use the Spectral Element Method to simulate wave propagation in an acoustic model that contains an isolated scatterer. The numerical example is in two dimensions, but it shows the same behavior as the theory derived above for three dimensions. The model parameters are given the following. Background velocity and density of the 1500 m by 1500 m model is 1000 kg/m^3 and 1500 m/s , respectively, and a single square scatterer (10 m by 10 m) is located in the origin. This scatterer has a velocity of 3000 m/s and a density of 2000 kg/m^3 . 720 sources are distributed evenly on a circle with a radius of 500 m from the center of the scatterer. The source wavelet is a Ricker wavelet with a central frequency of 50 Hz. In the Spectral Element Method, we use Lagrange polynomials of degree $N=4$ to interpolate the wave field in each quadrangular cell; the total number of spectral-elements is 90601. The time step used in the explicit integration scheme is $\Delta t = 0.1 \text{ ms}$ and we propagate the signal for 0.53 s. The wave field is recorded at two receivers $\mathbf{r}_A = (900, 750)$

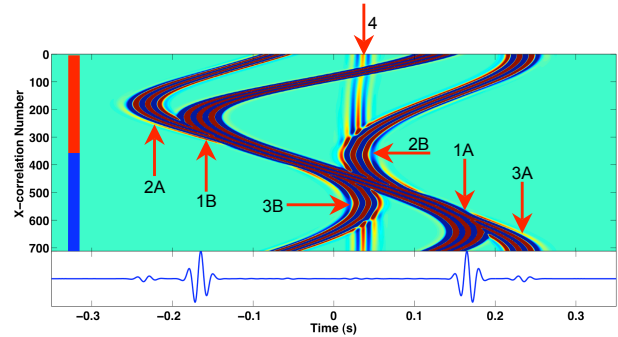


Figure 5. Top panel: cross-correlation of the waves recorded at the receivers as a function of time (horizontal axis) and source number (vertical axis) where the sources are numbered counterclockwise from east. The labels at the stationary points are the same as in figure 3. The color bar on the left side in the upper panel indicates the subsets of sources used in figure 6. Bottom panel: the cross-correlations after summation over all sources.

and $\mathbf{r}_B = (750, 950)$. The geometry of the experiment is drawn in Figure 4, indicating that $G(\mathbf{r}_A, \mathbf{r}_B)$ contains a direct arrival at $t \approx 0.17 \text{ s}$, and a scattered event at $\approx 0.23 \text{ s}$.

The top panel of Figure 5 contains the cross-correlations of the waves recorded at \mathbf{r}_B with \mathbf{r}_A , for each source. The bottom panel displays the sum of the cross-correlations over all sources. The sinusoidal features in the top panel are the causal and a-causal direct and scattered events with stationary points around $t \approx \pm 0.17 \text{ s}$, and $t \approx \pm 0.23 \text{ s}$, respectively. For example, the stationary point 1A gives the causal direct wave arriving at $t \approx 0.17 \text{ s}$, while the stationary point 1B gives the a-causal direct wave at $t \approx -0.17 \text{ s}$. Similarly, the stationary points 2A and 3A gives the causal and a-causal scattered waves arriving at $t \approx \pm 0.23 \text{ s}$. Of special interest is the arrival, marked with the label “4” at a constant travel time of about 0.03 s. This is the spurious arrival described in the previous sections. This spurious arrival is canceled by the contribution of the stationary points 2B and 3B. Indeed, there is no spurious arrival in the bottom panel at arrival time 0.03 s.

This numerical example thus confirms that the spurious arrival vanishes because of the destructive interference of the wave with constant arrival time (marked with the label “4”) with two stationary phase contributions 2B and 3B. Note that in this example we did not specify the scattering amplitude $f_k(\hat{\mathbf{n}}, \hat{\mathbf{n}}')$. Its properties are implicitly accounted for by the spectral element code.

In figure 6 we show the sum (in red) over the sources located along the lower half of the circle, and the sum (in blue) over the sources in the upper half circle. The sources along the lower half circle show the causal direct wave at $t \approx 0.17 \text{ s}$ and the causal scattered wave at $t \approx 0.23 \text{ s}$, but not their a-causal counterparts. The

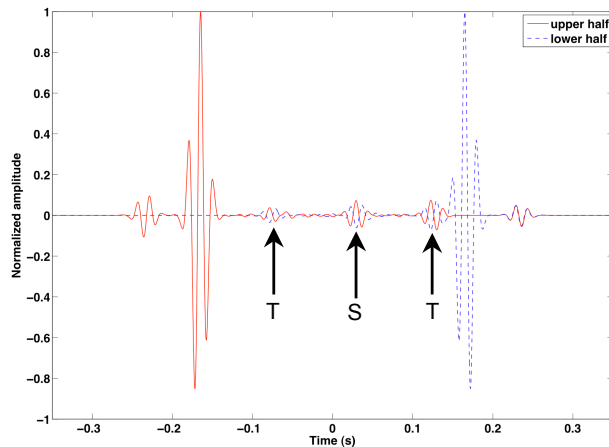


Figure 6. The cross correlations of figure 5. Solid (red) trace: sum over all the sources along the lower half circle. Dashed (blue) trace: sum over the sources along the upper half circle. The spurious arrival is marked with the label “S”, while truncation phases are marked with the label “T.”

reason is that the sources on the lower half circle only launch direct and scattered waves that propagate from receiver *A* to receiver *B*. The sources along the upper half circle launch waves in the reverse direction, and give the a-causal direct and scattered waves shown in blue.

The spurious arrival is marked with the label “S”. Both subsets of sources give a nonzero spurious arrival. The contribution from the sources at the lower half mostly contribute to the constant-time arrival marked with “4” in figure 5, while the sources from the lower half mostly contribute to the stationary phase points 2B and 3B in figure 5. As shown in figure 6, each of these contributions is nonzero, but they do cancel when summed. The abrupt truncation of the sum over sources leads to additional truncation phases marked with “T”, that individually are non-zero, but whose sum vanishes as well. Truncation phases result from the dominant endpoint contributions of oscillatory integrals [Bender & Orszag, 1978], and are a known complication in modeling waveforms with the reflectivity method [Burdick & Orcutt, 1979]. Truncation phases also occurred in field application of the extraction of the Green’s function from ocean-bottom seismic data [Mehta *et al.*, 2008]. Note that the arrival time of the truncation phases depends on the employed sources, while the arrival time of the spurious arrival is the same for every truncated source distribution. Also, the truncated phases can be suppressed by suitable tapering of the source strength, but this does not suppress the spurious arrival.

5 CONCLUSION

This work has two implications. First, the comparison of expressions (2) and (17) shows that the generalized

optical theorem holds. This work thus constitutes an alternative derivation of the generalized optical theorem, although Heisenberg’s original derivation [Heisenberg, 1943], which was based on the unitarity of the scattering matrix, is much simpler.

The second implication of this work is that, as shown in figure 6, for a limited source aperture the spurious arrivals do not vanish. This is the same phenomenon as the spurious arrivals that arise through cross-terms of single reflected waves from different layers in the subsurface [Snieder *et al.*, 2006]. In seismic applications, those cross-terms could be misinterpreted as reflectors in the subsurface.

From a practical point of view the spurious arrivals, as those shown in figure 6, are undesirable because these waves could be mistaken for true physical waves that are part of the Green’s function. One should be aware of these spurious arrivals whenever the source distribution used for the extraction of the Green’s function does not fulfill theoretical requirements.

ACKNOWLEDGMENTS.

This work grew out of a dinner conversation with our much appreciated friend and colleague Rodney Calvert. We thank Dimitri Komatitsch and Jeroen Tromp for their spectral-element codes and for instructing us in their use.

REFERENCES

- Bakulin, A., & Calvert, R. 2006. The virtual source method: Theory and case study. *Geophysics*, **71**, S1139–S1150.
- Bender, C.M., & Orszag, S.A. 1978. *Advanced Mathematical Methods for Scientists and Engineers*. New York: McGraw-Hill.
- Bleistein, N., & Handelsman, R.A. 1975. *Asymptotic expansions of integrals*. New York: Dover.
- Burdick, L.J., & Orcutt, J.A. 1979. A comparison of the generalized ray and reflectivity methods of waveform synthesis. *Geophys. J. Int.*, **58**, 261–278.
- Curtis, A., Gerstoft, P., Sato, H., Snieder, R., & Wapenaar, K. 2006. Seismic interferometry – turning noise into signal. *The Leading Edge*, **25**, 1082–1092.
- Faccioli, E., Maggio, F., Paolucci, R., & Quarteroni, A. 1997. 2D and 3D elastic wave propagation by a pseudo-spectral domain decomposition method. *J. of Seismology*, **1**, 237–251.
- Glauber, R., & Schomaker, V. 1953. The theory of electron diffraction. *Phys. Rev.*, **89**, 667–671.
- Heisenberg, W. 1943. Die “beobachtbaren Größen” in der Theorie der Elementarteilchen. *Z. Phys.*, **120**, 513–538.
- Hornby, B.E., & Yu, J. 2007. Interferometric imaging of a salt flank using walkaway VSP data. *The Leading Edge*, **26**, 760–763.
- Komatitsch, D., & Tromp, J. 2002. Spectral-element simulations of global seismic wave propagation-I. Validation. *Geophysical Journal International*, **150**, 390–412.

Komatitsch, D., Ritsema, J., & Tromp, J. 2002. The spectral-element method, Beowulf computing, and global seismology. *Science*, **298**, 1737–1742.

Larose, E., Margerin, L., Derode, A., van Tiggelen, B., Campillo, M., Shapiro, N., Paul, A., Stehly, L., & Tanter, M. 2006. Correlation of random wavefields: an interdisciplinary review. *Geophysics*, **71**, SI11–SI21.

Lobkis, O.I., & Weaver, R.L. 2001. On the emergence of the Green's function in the correlations of a diffuse field. *J. Acoust. Soc. Am.*, **110**, 3011–3017.

Mehta, K., Snieder, R., & Graizer, V. 2007. Downhole receiver function: a case study. *Bull. Seismol. Soc. Am.*, **97**, 1396–1403.

Mehta, K., Snieder, R., Calvert, R., & Sheiman, J. 2008. Acquisition geometry requirements for generating virtual source data. *The Leading Edge*, in press.

Priolo, E., Carcione, J. M., & Seriani, G. 1994. Numerical simulations of interface waves by high-order spectral modeling techniques. *J. Acoust. Soc. Am.*, **95**, 681–693.

Sabra, K.G., Gerstoft, P., Roux, P., Kuperman, W.A., & Fehler, M.C. 2005. Surface wave tomography from microseisms in Southern California. *Geophys. Res. Lett.*, **32**, L14311, doi:10.1029/2005GL023155.

Sabra, K.G., Conti, S., Roux, P., & Kuperman, W.A. 2007. Passive in-vivo Elastography from Skeletal Muscle Noise. *Appl. Phys. Lett.*, **90**, 194101.

Sabra, K.G., Srivastava, A., di Scalea, F.L., Bartoli, I., Rizzo, P., & Conti, S. 2008. Structural health monitoring by extraction of coherent guided waves from diffuse fields. *J. Acoust. Soc. Am.*, **123**.

Schiff, L.I. 1968. *Quantum mechanics*. 3rd edn. New York: McGraw-Hill.

Shapiro, N.M., Campillo, M., Stehly, L., & Ritzwoller, M.H. 2005. High-resolution surface-wave tomography from ambient seismic noise. *Science*, **307**, 1615–1618.

Snieder, R., & Şafak, E. 2006. Extracting the building response using seismic interferometry; theory and application to the Millikan Library in Pasadena, California. *Bull. Seismol. Soc. Am.*, **96**, 586–598.

Snieder, R., Wapenaar, K., & Larner, K. 2006. Spurious multiples in seismic interferometry of primaries. *Geophysics*, **71**, SI111–SI124.

Snieder, R., Wapenaar, K., & Wegler, U. 2007. Unified Green's function retrieval by cross-correlation; connection with energy principles. *Phys. Rev. E*, **75**, 036103.

van de Hulst, H.C. 1949. On the Attenuation of Plane Waves by Obstacles of Arbitrary Size and Form. *Physica*, **15**, 740–746.

van Wijk, Kasper. 2006. On estimating the impulse response between receivers in a controlled ultrasonic experiment. *Geophysics*, **71**(4), SI79–SI84.

Wapenaar, K., Fokkema, J., & Snieder, R. 2005. Retrieving the Green's function by cross-correlation: a comparison of approaches. *J. Acoust. Soc. Am.*, **118**, 2783–2786.

Wapenaar, K., Slob, E., & Snieder, R. 2006. Unified Green's function retrieval by cross-correlation. *Phys. Rev. Lett.*, **97**, 234301.

Wapenaar, Kees, & Fokkema, Jacob. 2006. Green's function representations for seismic interferometry. *Geophysics*, **71**(4), SI33–SI46.

Weaver, R.L. 2008. Ward identities and the retrieval of Green's functions in the correlations of a diffuse field. *Wave Motion*, in press,

<http://dx.doi.org/10.1016/j.wavemoti.2007.07.007>.

Weaver, R.L., & Lobkis, O.I. 2001. Ultrasonics without a source: Thermal fluctuation correlations and MHz frequencies. *Phys. Rev. Lett.*, **87**, 134301.

Weaver, R.L., & Lobkis, O.I. 2004. Diffuse fields in open systems and the emergence of the Green's function. *J. Acoust. Soc. Am.*, **116**, 2731–2734.

APPENDIX A: EVALUATION OF THE STATIONARY PHASE INTEGRALS

This section features details of the various stationary phase integrations starting with term $T1$ in equation (8). Using the vectors in expression (6), the length L_1 of equation (9) is given by

$$\begin{aligned} L_1 &= \cos \varphi \sin \theta (r_B \sin \theta_B - r_A \sin \theta_A) \\ &+ \cos \theta (r_B \cos \theta_B - r_A \sin \theta_A) \\ &= (x_B - x_A) \cos \varphi \sin \theta + (z_B - z_A) \cos \theta . \end{aligned} \quad (A1)$$

The integration is over the angles θ and φ and the stationary points are determined by the conditions

$$\frac{\partial L_1}{\partial \varphi} = -(x_B - x_A) \sin \varphi \sin \theta = 0 , \quad (A2)$$

$$\frac{\partial L_1}{\partial \theta} = (x_B - x_A) \cos \varphi \cos \theta - (z_B - z_A) \sin \theta = 0 . \quad (A3)$$

These expressions determine the angles θ_s and φ_s for which the phase of term $T1$ is stationary. The first condition gives $\sin \varphi_s = 0$, hence the stationary points are located in the (x, z) -plane.

In the following we treat the stationary point $\varphi_s = 0$, the contribution of the stationary point $\varphi_s = \pi$ follows by complex conjugation. For $\varphi_s = 0$, expression (A3) gives

$$\tan \theta_s = \frac{x_B - x_A}{z_B - z_A} . \quad (A4)$$

This angle is depicted in figure A1 where it can be seen that the stationary phase point is aligned with the points \mathbf{r}_A and \mathbf{r}_B .

Differentiation of expression (A3), and using the geometry of figure A1, gives for the second derivative at the stationary phase point

$$\begin{aligned} \frac{\partial^2 L_1}{\partial \theta^2} &= -(x_B - x_A) \sin \theta_s - (z_B - z_A) \cos \theta_s \\ &= -(x_B - x_A) \frac{x_B - x_A}{|\mathbf{r}_B - \mathbf{r}_A|} - (z_B - z_A) \frac{z_B - z_A}{|\mathbf{r}_B - \mathbf{r}_A|} \\ &= -|\mathbf{r}_B - \mathbf{r}_A| . \end{aligned} \quad (A5)$$

Differentiation of expression (A2) gives at the stationary

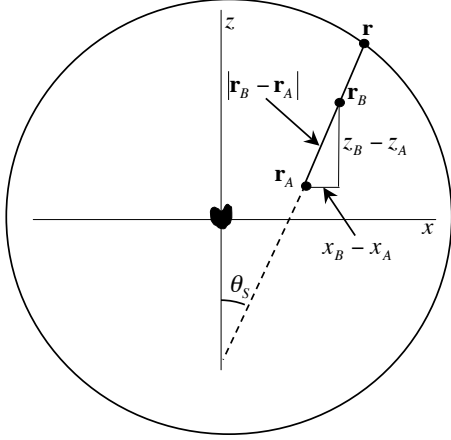


Figure A1. Geometric variables for the stationary phase analysis of term T_{1A} .

point

$$\frac{\partial^2 L_1}{\partial \varphi^2} = (x_B - x_A) \sin \theta_s . \quad (\text{A6})$$

For this stationary term, and all other terms, the mixed derivative vanishes at the stationary phase point:

$$\frac{\partial^2 L_1}{\partial \theta \partial \varphi} = 0 . \quad (\text{A7})$$

It follows from the geometry of figure A1 that at the stationary phase point

$$L_1 = |\mathbf{r} - \mathbf{r}_A| - |\mathbf{r} - \mathbf{r}_B| = |\mathbf{r}_A - \mathbf{r}_B| . \quad (\text{A8})$$

The stationary phase approximation of the θ - and φ -integration applied to the term T_1 of expression (8) gives [Bleistein & Handelsman, 1975; Bender & Orszag, 1978]

$$\begin{aligned} T_{1A} &= \frac{\rho^2}{(4\pi)^2} \exp(ik|\mathbf{r}_A - \mathbf{r}_B|) \\ &\times \left(e^{-i\pi/4} \right)^2 \sqrt{\frac{2\pi}{k|\partial^2 L_1/\partial \theta^2|}} \sqrt{\frac{2\pi}{k|\partial^2 L_1/\partial \varphi^2|}} \sin \theta_s . \end{aligned} \quad (\text{A9})$$

The factors $\exp(-i\pi/4)$ arise because the second derivatives both are negative. The $\sin \theta_s$ term comes from the Jacobian in the angular integration. With expressions (A5) and (A6) term T_{1A} reduces to

$$T_{1A} = -\frac{i\rho^2 \exp(ik|\mathbf{r}_A - \mathbf{r}_B|)}{8\pi k} \frac{\sin \theta_s}{\sqrt{|\mathbf{r}_A - \mathbf{r}_B|} \sqrt{\sin \theta_s |x_A - x_B|}} . \quad (\text{A10})$$

As shown in figure A1, $\sin \theta_s = (x_B - x_A)/|\mathbf{r}_A - \mathbf{r}_B|$. Inserting this in expression (A10) gives equation (12). Term T_{1B} in equation (13) follows by complex conjugation.

Next we treat the contribution of point 2A to term

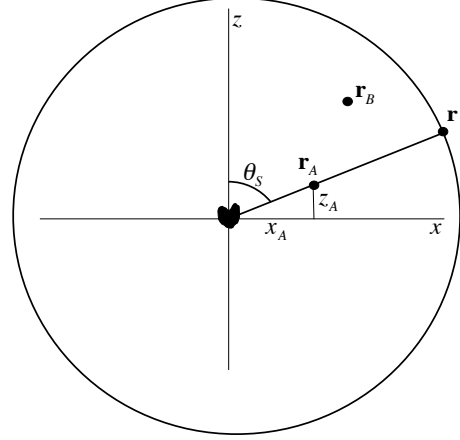


Figure A2. Geometric variables for the stationary phase analysis of term T_{2A} .

T_2 of expression (8). Using expression (6), the length L_2 is given by

$$\begin{aligned} L_2 &= -r_A \cos \varphi \sin \theta \sin \theta_A - r_A \cos \theta \sin \theta_A - r_B \\ &= -x_A \cos \varphi \sin \theta - z_A \cos \theta - r_B . \end{aligned} \quad (\text{A11})$$

The stationary phase condition for the angle φ gives $\partial L_2/\partial \varphi = x_A \sin \varphi \sin \theta = 0$, which implies that the stationary point lies in the (x, z) -plane: $\sin \varphi_s = 0$. We first analyze the point $\varphi_s = 0$. For this point, the stationary phase condition for the variable θ is: $\partial L_2/\partial \theta = -x_A \cos \theta + z_A \sin \theta = 0$. This gives the stationary point

$$\tan \theta_s = \frac{x_A}{z_A} . \quad (\text{A12})$$

This stationary phase point is sketched in figure A2. An analysis similar as for term T_1 shows that at this stationary point: $L_2 = -r_A - r_B$, $\hat{\mathbf{r}} = -\hat{\mathbf{r}}_A$, $\partial^2 L_2/\partial \theta^2 = r_A$, and $\partial^2 L_2/\partial \varphi^2 = x_A \sin \theta_s$. The stationary phase contribution from point 2A to term T_2 of expression (8) thus is given by

$$T_{2A} = \frac{i\rho^2 \exp(-ik(r_A + r_B))}{8\pi k} \frac{f^*(\hat{\mathbf{r}}_B, -\hat{\mathbf{r}}_A)}{r_B \sqrt{r_A}} \frac{\sin \theta_s}{\sqrt{\sin \theta_s x_A}} . \quad (\text{A13})$$

According to figure A2, $x_A = r_A \sin \theta_s$, which leads to expression (14).

The stationary phase point 2B corresponds to $\varphi_s = \pi$. The stationary phase condition for θ is in this case $\partial L_2/\partial \theta = x_A \cos \theta + z_A \sin \theta = 0$. This gives the stationary point

$$\tan \theta_s = -\frac{x_A}{z_A} . \quad (\text{A14})$$

This point is sketched in figure A3. Using that $\theta_s = \pi - \theta_A$ it follows that at this stationary point: $L_2 = r_A - r_B$, $\hat{\mathbf{r}} = \hat{\mathbf{r}}_A$, $\partial^2 L_2/\partial \theta^2 = -r_A$, and $\partial L_2/\partial \varphi^2 = -x_A \sin \theta_A$.

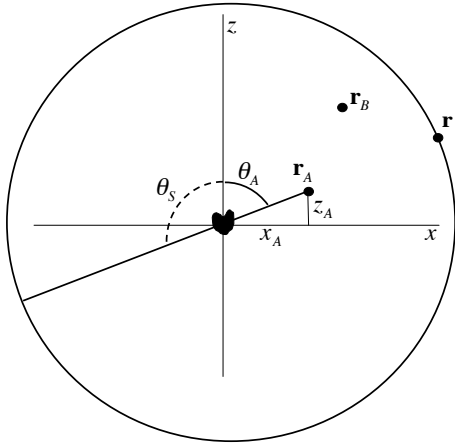


Figure A3. Geometric variables for the stationary phase analysis of term T_{2B} .

The stationary phase contribution of this point is thus given by

$$T_{2A} = -\frac{i\rho^2}{8\pi k} \frac{\exp(ik(r_A - r_B))}{r_B \sqrt{r_A}} f^*(\hat{\mathbf{r}}_B, \hat{\mathbf{r}}_A) \frac{\sin \theta_A}{\sqrt{\sin \theta_s x_A}} . \tag{A15}$$

Using the geometric relation $\sin \theta_A = x_A/r_A$ reduces expression (A15) to equation (15).

